PRECISION
RAMAN

Best-in-class Raman microscopes
for research and analytical requirements
backed with world-class customer
support and service.

edinst.com

RESEARCH ARTICLE

Journal of **RAMAN SPECTROSCOPY** WILEY

Development of a gas-phase Raman instrument using a hollow core anti-resonant tubular fibre

William S.M. Brooks[1] | **Matthew Partridge**[2] | **Ian A.K. Davidson**[2] | **Charles Warren**[1] | **George Rushton**[3] | **Joseph Large**[3] | **Michael Wharton**[3] | **Jonathan Storey**[1] | **Natalie V. Wheeler**[2] | **Michael J. Foster**[1]

[1]IS-Instruments, Pipers Business Centre, Tonbridge, UK

[2]Optoelectronics Research Centre (ORC), Zepler Institute for Photonics and Nanoelectronics, University of Southampton, Southampton, UK

[3]Jacobs Clean Energy, Specialist Consultancy and Laboratory Solutions, Warrington, UK

Correspondence
William S.M. Brooks, IS-Instruments, Pipers Business Centre, 220 Vale Road, Tonbridge, TN9 1SP, UK.
Email: wbrooks@is-instruments.com

Funding information
Innovate UK, Grant/Award Number: 103973

Abstract

Versatile and flexible gas analysis for compositional identification and quantification is a demand found in a variety of diverse sectors. As such, a compact, deployable instrument exhibiting both high specificity and sensitivity is a highly attractive proposition for a wide range of applications. In this paper, we describe a gas phase Raman spectroscopy-based device using state-of-the-art anti-resonant (tubular) hollow core micro-structured optical fibre (HC-MOF). This fibre architecture allows the use of lengths that are typically longer than have been demonstrated previously, allowing substantially enhanced interaction lengths between the pump laser and the gas sample to be achieved, addressing the sensitivity challenges typically observed in gas-phase Raman measurements and enabling application for remote sensing in hazardous environments. We describe the successful development of a compact, fibre-integrated instrument and present results obtained during a test campaign at an industrial laboratory; marking a milestone in gas-phase Raman spectroscopy. The unique properties of the MOF used allowed a 20-m length to be utilised, representing a new record length for gas phase Raman measurements. The identification and quantification of a variety of gas species, ranging from simple homonuclear diatomic gases to heteronuclear organic gas species were achieved, and, building on previous studies, the instruments stability, gas concentration linearity response, and the hollow core fibre filling and purging characteristics were investigated.

KEYWORDS
fibre-enhanced gas Raman, hollow core anti-resonant tubular fibre, industrial application, multi-species detection

1 | INTRODUCTION

Gas sample compositional analysis is routinely required across a range of industries including the oil and gas, nuclear and environmental sectors. These measurements are commonly completed using gas chromatographic (GC) separation methods coupled with a variety of gas-specific detectors such as thermal conductivity and flame ionisation detectors. Although broadly effective, these systems are typically complex, expensive and demand ex-situ operation where gas samples must be physically obtained and taken to an off-site laboratory for characterisation or additional pipework has to be introduced to allow gas flow to an off-site location. GC instruments can achieve high detection sensitivity levels[1]; however, the technique suffers from low selectivity due to the requirement for gas specific separation columns and detectors. For example, hydrogen detection is typically accomplished via a dedicated molecular sieve column, helium carrier gas and thermal conductivity detector.[2] In this configuration, to simultaneously monitor other gas species, such as methane and ethane, would demand additional columns, carrier gases (e.g., argon) and detectors. If further gas species are targeted, the GC instrumentation becomes increasingly complex, bulky and expensive. Consequently, alternative gas metrology methods are a fertile research area.

The high selectivity inherent to Raman spectroscopy offers excellent opportunities for quantitative compositional analysis of materials. The technique has demonstrated versatility through deployment in diverse applications ranging from laboratory based fine chemicals characterisation[3] to in-situ industrial process monitoring.[4] However, the Raman effect is a weak process[5] and so measurements typically suffer from low sensitivity, therefore most Raman applications target samples with high Raman scattering centre densities. Equation 1 illustrates this principle:

$$I = I_0 E_\lambda N \sigma \Omega L \qquad (1)$$

where I is the Raman signal intensity, I_0 is the laser power, E_λ is the instrument efficiency, N is the number density, σ is the Raman cross-section, Ω is the scattering solid angle, and L is the laser-sample interaction length. In practice, this results in Raman measurements being predominantly used for analysis of solid and liquid samples.

Gas samples are inherently diffuse and therefore Raman signal capture is made substantially more challenging. Methods to facilitate these measurements include sample pressurisation (increasing N), increasing the laser power (I_0) or increasing the interaction path-

length between the Raman excitation source and target gas molecules (increasing L), or indeed a combination of these methods. Sample pressurisation assemblies have been demonstrated in the oil and gas industry where a confocal optical probe design has interrogated a target gas sample via a sapphire optical window.[6] A variety of approaches aimed at increasing the optical path-length through the target gas sample have also been trialled. These include methods where the gas sample is introduced in to (a) an optical cavity where a series of mirrors guides the Raman excitation light through an increased pathlength[7] and (b) hollow core waveguide methods, where a gas sample is introduced into the hollow region of a waveguide which guides the light through an increased interaction path through the gas sample. These include glass capillary or metal 'light-pipe' methods[8]; and hollow core fibre optic based methods which operate via novel light guiding mechanisms.[9–11]

Despite the well documented advantages that Raman based gas detection systems potentially offer, no single method appears to have been widely adopted by the gas sensing community, this may be related to sample handling constraints, and/or complex optical alignment requirements which limit use to static, bench-top based environments.

In this paper, we present the development of a commercially viable Raman prototype instrument exploiting a fibre-based approach where the optical interaction path length is dramatically increased by incorporating a 20-m tubular hollow-core antiresonant fibre into the system.[12] This component consequently fulfils the gas sampling function of the instrument, itself tailored to detect a broad range of gas species of potential interest to multiple industrial sectors.

Hollow core microstructured fibres (HC-MOFs)[13,14] are a specialty type of optical fibre where light is guided in a hollow core. HC-MOFs provide low loss and low bend sensitivity and can be fabricated in long lengths (>100 m); making them very attractive as a gas cell for Raman spectroscopy. Furthermore, recent fabrication advances are moving them ever closer to a viable commercial technology.[11]

To date, Raman gas sensing using HC-MOFs has been predominantly carried out using hollow core photonic bandgap fibres and the lowest demonstrated limit of detection is 0.2 ppm for methane gas, using a 2 W laser, with the gas sample at 20 bar.[10] In recent years, a different type of HC-MOF has emerged, known as hollow core antiresonant fibre (HC-ARF), due to its guidance mechanism. The first demonstration of HC-ARF for use in Raman gas sensing was reported in 2017,[15] highlighting that HC-ARF can potentially provide several advantages for Raman-based gas sensing, including lower fibre

attenuation, more than an order of magnitude lower overlap between the guided light and the silica microstructured cladding and larger core sizes (which can reduce gas filling time). More recent work[16] further demonstrated these features and showed a limit of detection of ~25 ppm for carbon dioxide gas, with 1.3-W laser power at 3.5-bar gas pressure. All reported works so far use fibre lengths of only a few metres; in HC-PBGFs this is limited by the fibre attenuation, whilst using HC-ARFs there is considerable scope to explore longer fibre lengths.

Gas phase Raman measurements using HC-MOFs have, to-date, typically been constrained to static, laboratory-based experiments, where often limit-of-detection (LoD) thresholds have been targeted.[17] Whilst detection of several different gas species has been demonstrated, for a variety of interesting applications (such as breath analysis[17] and fruit ripening[18]), deployment for in-situ gas characterisation has not been possible. In this work, a system has been successfully assembled, tested and validated and then subsequently deployed to an industrial laboratory for performance testing. This demonstrates the reality of a compact, integrated, stable, site-deployable gas phase Raman instrument capable of simultaneous detection of multiple gas species with applications across a broad range of industrial and academic sectors. This work therefore differentiates from existing HC-MOF based systems where extended optical arrangements, using short fibre lengths have been demonstrated.

Initially, the instrument functionality was established via characterisation of ambient atmospheric gas species. The Raman signal stability and gas fill/purge times and characteristics were assessed. A demonstration of simultaneous multi-species detection is presented, where component species concentrations varied between 0.04% and >99%. The Raman signal response linearity across a range of target concentrations is presented. The instrument was shown to characterise a variety of gas species ranging from simple homonuclear diatomic molecules to more complex heteronuclear organic gas species.

2 | INSTRUMENT

2.1 | Concept

An integrated, free-space coupled design was developed. This allowed for a compact instrument configuration and easy optical alignment, whilst maximising efficiency. This integrated solution is shown schematically in Figure 1. The design comprised of three subsystems:

1. Czerny-Turner (CT) monochromator-type spectrometer
2. 532 nm laser and launch/coupling optics
3. Tubular hollow-core anti-resonant fibre (HC-ARF)

The system included a series of spatial and optical filters to ensure full optical separation between the laser and the spectrometer was achieved. This ensured the incidence of stray laser light on to the spectrometer CCD was minimised, thereby enhancing system performance by reducing a significant noise contribution. Figure 1 also indicates optical filter positions, where the long pass (LP) filter blocks 532-nm laser light from entering into the spectrometer and the laser line (LL) filter suppresses additional laser wavelengths which the laser may produce.

2.2 | Hollow core microstructured optical fibre

The hollow core fibre was designed and fabricated by the Optoelectronic Research Centre (ORC) at the University
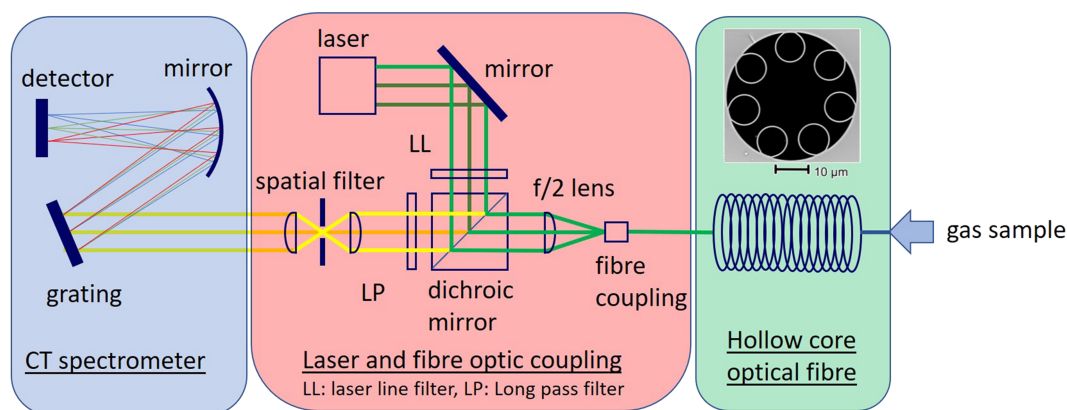

FIGURE 1 Integrated design gas phase Raman instrument configuration [Colour figure can be viewed at wileyonlinelibrary.com]

of Southampton, UK. Two fibre design options were considered (a) a hollow core—photonic band gap fibre (HC-PBGF) and (b) a hollow core—anti-resonant fibre (HC-ARF). Each fibre presents advantages specific to particular applications, for example HC-PBGFs exhibit negligible bend losses and usually have a higher numerical aperture (NA) than HC-ARFs,[19] leading to higher capture efficiency. Therefore, HC-PBGFs may be best suited for applications which demand short fibre lengths and a compact device; where the fibre may need to be tightly coiled. HC-ARFs allow for more varied design options[20] including larger core sizes and greater optical bandwidth; they also have multiple transmission windows and can have lower attenuation compared to HC-PBGFs,[21] especially at visible and NIR wavelengths relevant to Raman spectroscopy.

Our goal was to demonstrate a compact and practical sensing unit which could be used in an industrial setting, outside of the confines of a well-controlled laboratory environment. Furthermore, we wanted to exploit the flexibility of the fibre to enable a system which could be used for remote access to hazardous areas. This system therefore required the use of a fibre length beyond that previously explored for Raman-based gas sensing using HC-MOFs. A 532-nm pump wavelength and a broad 400–4500 cm^{-1} Raman spectral range were identified as being necessary to enable simultaneous identification and quantification of multiple target gas species. The long fibre length combined with the multispecies detection requirement resulted in a need for a HC-MOF with a broad, low loss transmission window at visible wavelengths. Additionally, the HC-MOF would need to be coilable; and also be able to navigate around obstructions, but not necessarily to extremely small bend diameters.

Following consideration of these factors, a tubular HC-ARF was selected as it best met these requirements and the application demands of a gas phase Raman system. The core diameter (∼21 μm) was chosen to best balance the competing effects of confinement loss and gas filling time (which both reduce for larger core sizes) and macro- and micro-bend losses, which increase for larger core sizes, and therefore limit the fibre's deployability due to handling and coiling related transmission losses.

A 20-m fibre length was selected to balance the competing system requirements of the gas fill time (which increases with the square of the fibre length[22]) and the increase in Raman signal which can be achieved with longer interaction path lengths. This length also expands the deployment options for the system, where, whilst designed to operate in a loosely coiled configuration in this investigation, could also be uncoiled and act as a remote gas 'sniffer' sensor. In this configuration, the main system hardware would be located at a fixed on-site location and the uncoiled HC-MOF gas sensor deployed to a target area. Furthermore, this type of fibre and length would also present the opportunity to form a sensor network by incorporating multiple fibres into the system to capture gas composition data from multiple target sites.

Figure 2a shows the transmission and loss of the fibre used in this work. The loss was measured by the traditional cutback method where the transmission of long (402 m) and short (100 m) lengths of the fibre were measured sequentially (with the optical launch
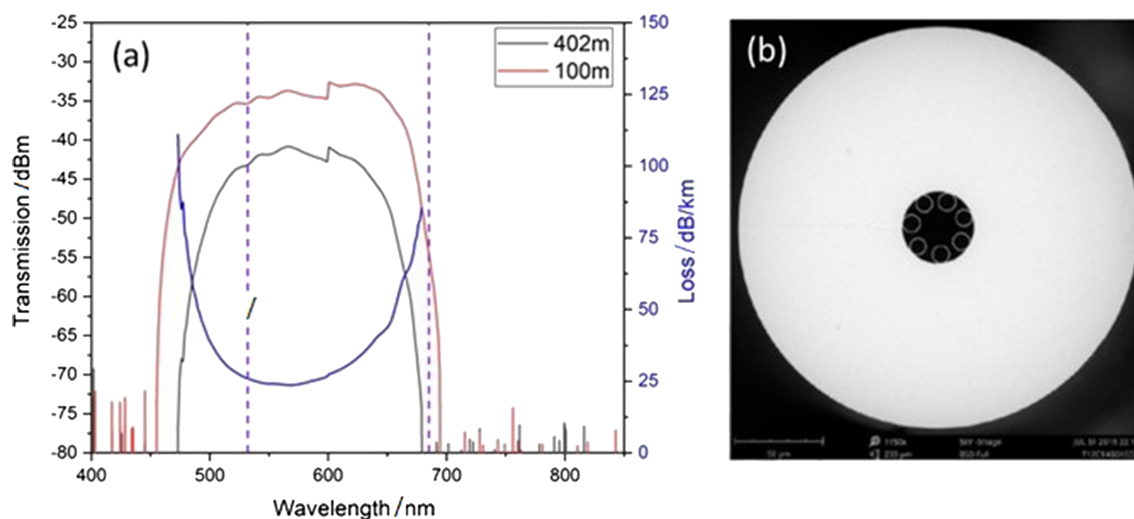

FIGURE 2 (a) Transmission and loss measurements of the tubular hollow core antiresonant fibre (HC-ARF) used in this work and (b) scanning electron microscope (SEM) image showing the fibres cross section (scale bar = 50 μm) [Colour figure can be viewed at wileyonlinelibrary.com]

maintained between measurements), and the loss deduced from these. The loss at the pump wavelength (532 nm) is ∼26 dB/km with the fibre exhibiting minimum loss of ∼23 dB/km at 569 nm, and sub-150 dB/km loss across the entire 400–4200 cm^{-1} measurement range. These losses, whilst not the absolute lowest achieved in a HC-MOF, are excellent at these wavelengths and are the reason long lengths of fibre can be used. Figure 2b is a scanning electron microscope (SEM) image of the HC-ARF cross-section showing the tubular core architecture. Further details of the fibre design and operational performance are described by Davidson et al.[21]

2.3 | Alignment and instrument configuration

Alignment of the HC-ARF to the internal optical hardware elements was found to be critical for overall system performance. In particular, stable optical coupling between the pump laser and the HC-ARF was essential, as any small drift in alignment will effectively change (reduce) the pump laser power reaching the gas sample and therefore reduce the generated Raman signal. This is challenging due to the 21-μm diameter of the fibre and therefore stable alignment at the micron-scale is required.

As shown in Figure 1, the laser was directed to the HC-MOF via a 90° turning mirror and a dichroic mirror. The laser spot diameter was estimated at 8.6 μm. The mode field diameter of the fundamental mode of the HC-MOF was estimated to be ∼14 μm.[23] This size mismatch indicates that some higher order modes were also likely launched into the fibre, further accounting for observed transmission loss variation.

Alignment optimisation between the pump laser and HC-ARF was achieved via coupling a power metre to the distal end of the fibre and monitoring power throughput whilst adjustment of the fibre mounted on an XYZ stage was completed. It was estimated, via operation of a

motorised XYZ translation stage, that XZ axis tolerance was approximately ±2 μm and the Y-axis (focus) tolerance was ±20 μm.

Figure 3 shows a labelled photograph of the full instrument assembled according to the configuration described in Figure 1. A Roithner LaserTechnik RLTMSL CW laser was selected as the Raman excitation source providing specifications in-line with the demands of the HC-ARF, including the single longitudinal mode requirement. This unit operated at $\lambda = 532 \pm 1$ nm with 200 mW output power. The laser power available to launch into the HC-MOF, after accounting for lens and filter transmission losses, was approximately 175–180 mW. The laser power at the fibre output, measured using a power metre, as described previously, was typically between 80 and 100 mW, resulting in 55–60% coupling/transmission efficiency. This indicates an opportunity for improvement and the highest power output achieved was 145 mW, corresponding to a coupling efficiency >80%.

An Andor iVac 316 camera was selected for the system detector; this provided good quantum efficiency over the target spectral range and excellent sensitivity. The system was designed to operate within a spectral range between 400- and 4500- and 6-cm^{-1} resolution. This ensured that a diverse range of gas species could be simultaneously detectable; for example from Cl_2 to H_2 with Raman shifts of 570 and 4150 cm^{-1}, respectively.

The prototype instrument shown in Figure 3 was operated during this phase of development without a full enclosure. This facilitated easy access for iterative alignment activities. The dimensions of the complete unit, including full enclosure would be approximately 500 (length) × 300 (width) × 200 (height) mm, excluding the laser power supply. There is considerable scope to further reduce the form factor of the unit, depending on precise application requirements. This could be accomplished via the incorporation of alternative detectors and/or laser heads. The availability of compact cage-
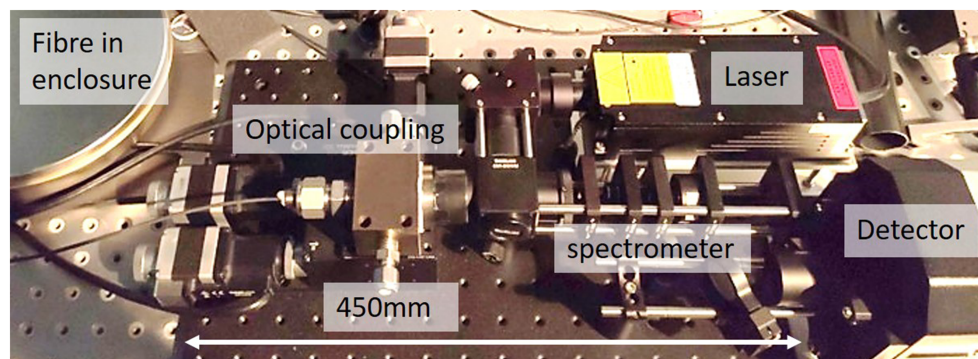

FIGURE 3 Image of instrument layout showing key sub-system components [Colour figure can be viewed at wileyonlinelibrary.com]

mounted optical coupling hardware will also further reduce the dimensions and mass of the system.

This paper presents results captured at ambient temperature from the following gas species: O_2, N_2 and H_2O (g) from ambient atmospheric samples and CO_2, CH_4 and C_3H_8 from commercially supplied bottled sources. Where gas dilution for mixed sample and variable concentration analysis was required, a G·A·S EasyCal Calibration System, with 0–100 ml range was used.

3 | RESULTS AND DISCUSSION

Instrument assembly, functional testing and initial validation was completed by IS-Instruments at company facilities in Tonbridge, UK. The system was then transported and deployed to the Jacobs Chemistry and Materials Laboratories in Warrington, UK, demonstrating the versatility of the instrument and potential for further site/field operation.

3.1 | Basic instrument functionality

Initial instrument functionality was confirmed via measurement of ambient atmospheric gases, principally N_2, O_2 and H_2O(g). These gas species also provided convenient and discreet peaks for alignment and wavelength calibration purposes. Figure 4 shows the raw Raman spectra obtained from an ambient atmospheric air sample. O_2, N_2 and H_2O are readily captured in single frame acquisition times of ~1 s. This initial
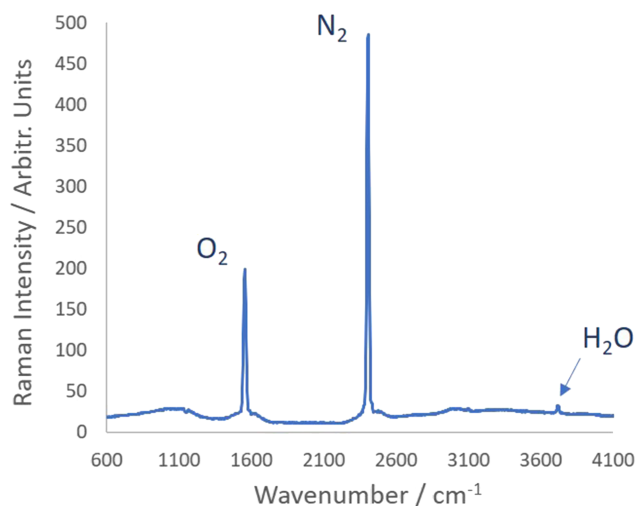

FIGURE 4 Raman spectra of ambient atmospheric air sample [Colour figure can be viewed at wileyonlinelibrary.com]

demonstration also highlighted the challenges associated with a free-space coupled design where eliminating both ambient light and residual scattered laser light from the detection elements of the system demanded the introduction of additional optical and spatial filters. This challenge is unique to an integrated instrument solution, differing from alternative and modular arrangements where each sub-system may be contained in independent enclosures. In addition to the discreet gas Raman peaks, Figure 4 (obtained after the additional filter fitting) shows a baseline signal that continues to indicate the presence of low broadband light levels and highlights the importance of comprehensive internal baffling and system enclosure. Accounting for Raman scattering cross-section, detector efficiency, grating efficiency and fibre loss (Figure 2), the peak heights of this spectrum were found to indicate an N_2:O_2 ratio close to known atmospheric composition. The observed deviation highlighted the importance of applying a white light correction routine to future iterations of the instruments to fully correct for wavelength dependent transmission variability and enable accurate quantification of multiple gases in a single sample. At this stage of the development, this result confirmed basic gas species detection and was used to identify where next phase efforts should be directed.

3.2 | Instrument stability

Initial stability testing of this type of tubular HC-MOF was examined by Partridge et al.[24] where power throughput and Raman peak characteristics were established. Due to practical constraints related to the deployment configuration, in this work the stability of the Raman response was monitored only. This was achieved via the capture of ambient atmospheric N_2 and O_2 spectra over a 4-h duration. Initially, Raman peak heights were assessed and compared to their respective area integrals, so as to determine an optimal metric. It was found that each case returned a near identical trend and therefore due to the ease with which the peak height could be determined, peak heights (whilst accounting for signal background) were the selected metric used throughout this investigation.

Figure 5 shows the O_2 and N_2 Raman peak heights tracked, presented at 30-min intervals throughout the 4-h period. The O_2 peak maintained a mean peak height at 172 ($\sigma = 4.3$, %$\sigma = 2.5$) and the N_2 peak maintained a mean peak height at 456 ($\sigma = 17.2$, %$\sigma = 3.8$). Each data point represents a single frame acquired in 1 s. Error bars were excluded due to small size. This was found to be in approximate agreement with predicted signal-to-noise ratio characteristics observed at different peak intensities.
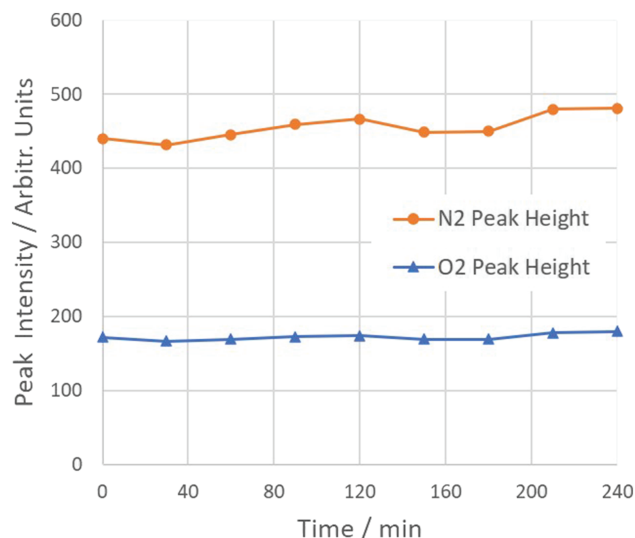
FIGURE 5 N_2 and O_2 peak height stability over 4-h duration [Colour figure can be viewed at wileyonlinelibrary.com]

FIGURE 7 Raman spectra of CO_2/N_2 sample captured at 26 min as shown in Figure 6 [Colour figure can be viewed at wileyonlinelibrary.com]
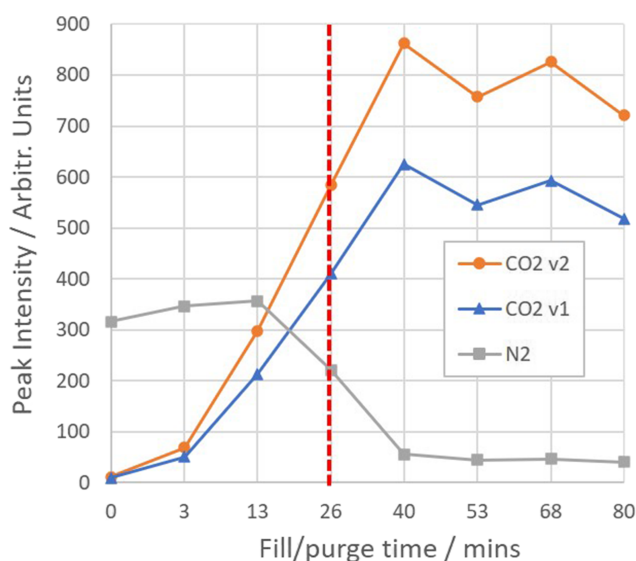

FIGURE 6 CO_2 v1 and v2 peaks and N_2 peak tracking over filling/purging 100-min duration [Colour figure can be viewed at wileyonlinelibrary.com]

FIGURE 8 Raman spectrum of gas mix containing 0.32% propane (C3H8), 3.68% methane (CH_4) and 96% carbon dioxide (CO_2) [Colour figure can be viewed at wileyonlinelibrary.com]

3.3 | Gas filling and purging

The gas filling and purging characteristics of the fibre were also of significant interest and considered central to the commercial viability of a deployable instrument. Gas flow dynamics in HC-MOFs have been investigated by several groups in recent years[25–27] and different dynamics have been identified depending on the gas pressure (and the subsequent mean free path of the gas molecules) and the fibre's geometry, specifically core diameter and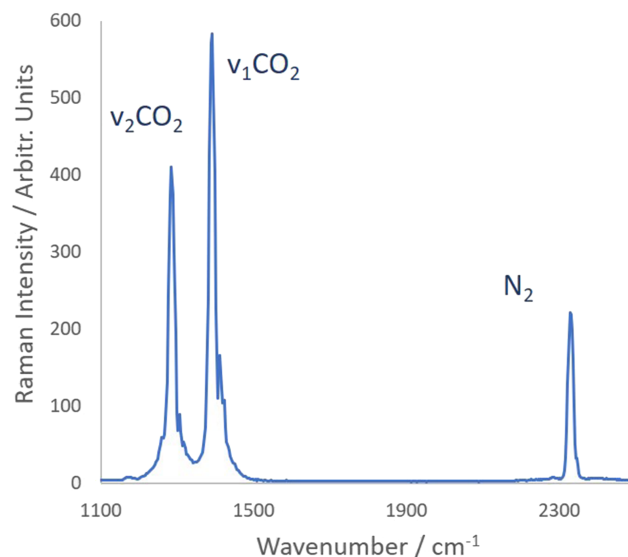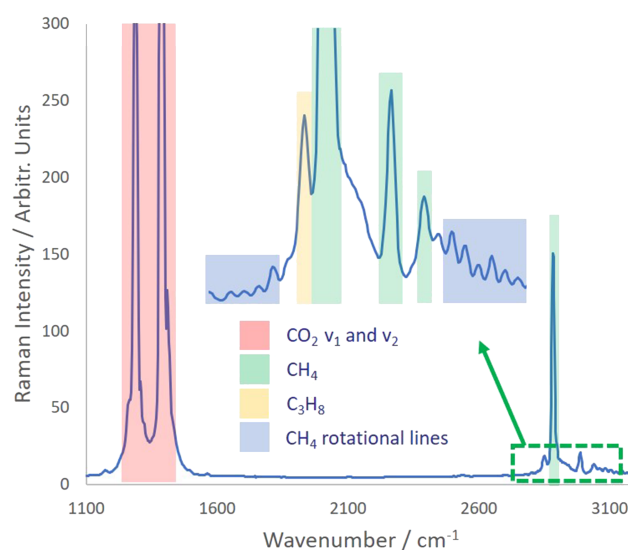 length. For the work shown here, gas fill, and accompanying purge times and characteristics were assessed by coupling the distal end of the fibre to a custom gas handling system which allowed the fibre to be filled with pressurised bottled gas. CO_2 was introduced to the fibre at a positive pressure differential of 2 bar. This was achieved by replacing a 0 bar gauge pressure at the fibre (1-bar absolute pressure) with a 2-bar gauge pressure (3-bar absolute pressure). This pressure regime was replicated for all results. Due to these filling conditions and as we are filling the fibre from one end, with the other end open to atmosphere, the pressure-driven

flow model described in Masum et al.[26] is a suitable choice for estimating the filling time, with the caveat that it does assume a circular core geometry, which differs from the tubular design used here. Using this model and the experimental conditions described, we estimated a filling time of ∼60 min.

Figure 6 shows Raman peak tracking of ambient atmospheric N_2 and pressurised bottled CO_2 v_1 and v_2 peaks as the CO_2 was introduced into the hollow core fibre, whilst simultaneously the N_2 was purged. The total tracking duration was 100 min. Each Raman spectra was obtained in 0.6 s, each data point corresponding to a single frame captured every 15 s. The CO_2 peaks become visible in <1-min fill time, whilst the N_2 peak maintained intensity (briefly increasing) for 13 min before reducing, indicating a latency time of the resident gas species. This observation may be caused by dead-space regions in the gas coupling pipework requiring longer purge durations to remove resident gas and/or an effect related to fibre end being open to the ambient atmosphere, the latter may also explain the persistence of N_2 throughout the

tracking duration. It is anticipated that this latency would be reduced with increasing gas sample pressure differential and future investigations will assess this characteristic.

Following a total 40-min fill time for the CO_2 sample, a relatively stable peak intensity was achieved, where the observed periodicity between 40 and 100 min may be caused by pressurisation differentials and/or laser power output variation (laser stability found to vary according to specification [<5%] contributing to observed Raman peak intensity variation). Simultaneously, the N_2 peak following a 13-min latency time, in which the peak actually increased, (which again may be due to localised pressurisation effects) and 27-min transition/purge time, produces a stable peak intensity level. The low-level peak intensity maintained after 40 min is likely due to residual N_2 present in the fibre and/or 'dead-space' in the gas pipework interface that may either require longer time-scales (or higher pressures) to fully purge. In the case of pipework 'dead-spaces', a dedicated purge valve located immediately prior to the fibre interface would facilitate rapid gas sample exchange and limit this observed effect.

The observed 40-min fill time is quicker than predicted using the model described by Masum et al.[26]; this could potentially be due to the non-circular core geometry of the tubular HC-MOF design, which has previously been shown to enable faster filling times as compared to circular core fibres.[28]

Figure 7 shows the Raman spectrum of the gas mixture captured after 26 min from the first introduction of the pressurised CO_2 sample. As indicated with a dashed line in Figure 6 this is at a time point where both gas species are readily identified; the CO_2 content and Raman signal increasing and the N_2 content and Raman signal decreasing.

3.4 | Propane, methane and CO_2 gas mix

The capture of Raman spectra of organic gas species was also conducted. Figure 8 shows the Raman spectra of a gas sample containing 0.32% propane, 3.68% methane and 96% carbon dioxide, introduced at a 2-bar pressure differential into the HC-ARF. The spectrum was captured in 60 × 1 s accumulations and clearly identifies each of
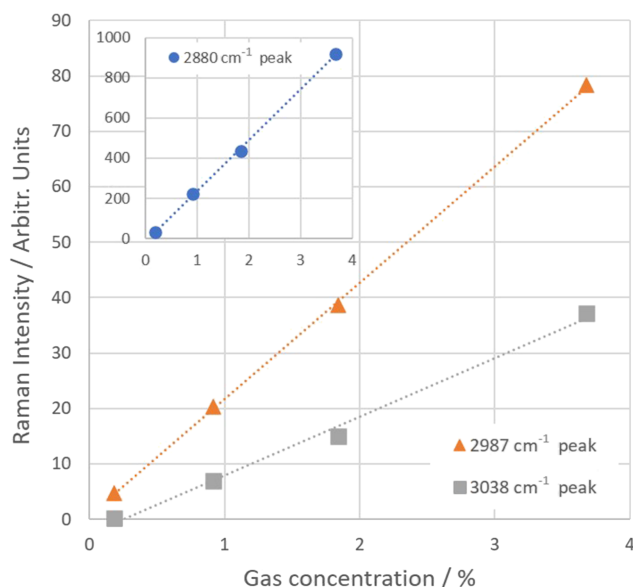
FIGURE 9 Methane Raman peak intensity versus concentration: A linearity response assessment. Linear trend lines for each plot are shown [Colour figure can be viewed at wileyonlinelibrary.com]

TABLE 1 Summary of gas sample composition

| | Gas species and concentration | | |
Sample	Methane, CH_4%	Ethane, C_2H_6%	Carbon dioxide, CO_2%
1	2	0.16	97.84
2	1.5	0.12	98.38
3	1	0.08	98.92
4	0.5	0.04	99.46

the three component gas species, as labelled. Additionally, the methane rotational Raman peaks are clearly visible as highlighted in Figure 8. This result emphasises the capacity of the instrument to capture multiple gas species simultaneously at substantially different partial pressures.

3.5 | Methane Raman peak linearity

A clear provision of the instrument was to quantitatively characterise target gas species. In this context, sequential and variable gas concentrations were introduced into the HC-ARF. Figure 9 shows a peak tracking graph where the three CH_4 Raman peaks identified in Figure 8 are
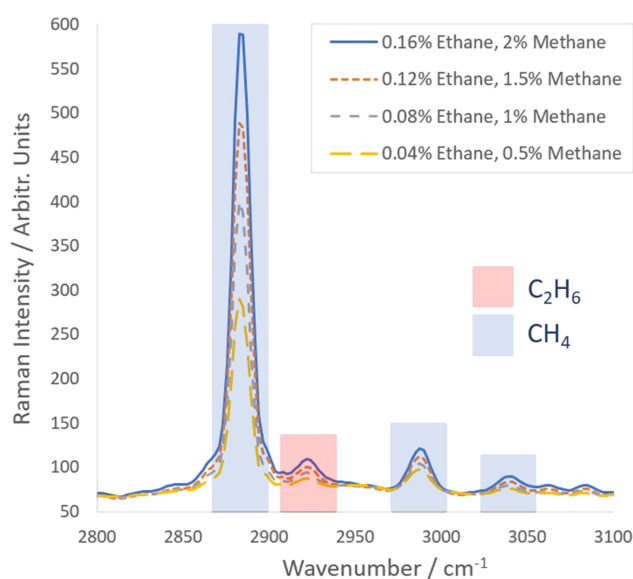
tracked as the methane gas concentration was varied from 0.184% to 3.68%, where the remaining sample comprised of CO_2. Error bars were excluded due to small size. R^2 values of 0.992 (2880-cm^{-1} peak), 0.993, (2987-cm^{-1} peak) and 0.9926 (3038-cm^{-1} peak) demonstrate excellent signal response linearity for all three CH_4 peaks over the gas concentrations investigated.

3.6 | Ethane/methane gas mix in CO_2

The sensitivity of the system to detect lower gas concentrations (<500 ppm) was also assessed. A series of ethane/methane mixes in CO_2 were investigated to confirm detection and quantification thresholds, where detection was confirmed via the identification of visible peaks and quantification confirmed via peak intensity versus gas species concentration linearity analysis, as shown in the previous section. The composition of the four samples analysed are shown in Table 1.

Figure 10 shows the Raman spectra of each of the samples 1–4 listed in Table 1. Each spectrum was captured in 60×1 s accumulations. Each of the three characteristic methane peaks identified previously are clearly visible as highlighted in Figure 10. Additionally, a unique ethane peak is identified at approximately 2920 cm^{-1}. As the concentration of each gas species reduces, a corresponding reduction in peak height is observed.

Figure 11a shows the signal response linearity of the methane peak at 2880 cm^{-1} as the gas concentration is varied between 0.5% and 2%. Error bars were excluded due to small size. Good linearity is observed with $R^2 = 0.9878$. Furthermore, the signal response linearity of the ethane peak as the gas concentration is varied between 0.04% and 0.16% is shown in Figure 11b, again good linearity is observed with $R^2 = 0.9954$. This result

FIGURE 10 Raman spectra of ethane and methane at concentrations as labelled [Colour figure can be viewed at wileyonlinelibrary.com]
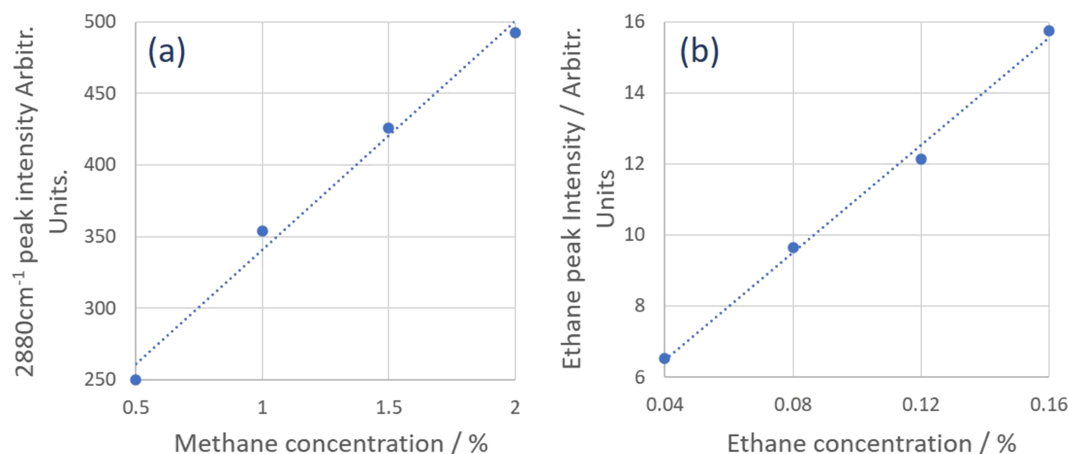

FIGURE 11 Raman peak intensity versus gas concentration plots: (a) methane 2880-cm^{-1} peak and (b) ethane peak. Linear trendlines for each plot are shown [Colour figure can be viewed at wileyonlinelibrary.com]

emphasises the capacity of the instrument to both identify *and* quantify multiple gas species simultaneously, at concentrations <0.05%.

The aim of this work was not to demonstrate record limit of detection but to develop a practical demonstrator, to move this sensing paradigm out of the lab and towards commercial deployment. Whilst evaluation of the limit of detection of this system will form part of our future work, the measurements above demonstrate detection of 400-ppm ethane, which is not far from the 25-ppm limit of detection demonstrated in Sieburg et al.[29] Within the system demonstrated here, there is significant room to improve the limit of detection (e.g., by increasing pump laser power and gas sample pressure) which could be exploited for applications which require higher sensitivity.

4 | CONCLUSIONS

Substantial progress towards the production, verification and validation of a site-deployable Raman based gas detector has been presented. The development of a purpose-built gas phase Raman instrument and key results are summarised. Initial validation of the design concept was completed via the successful characterisation of ambient atmospheric air gas species: N_2, O_2 and $H_2O(g)$. Each of the characteristic Raman peaks associated with each gas species was readily identified. The stability of the instrument was assessed, providing a crucial benchmark for subsequent gas quantification analysis. The hollow core fibre fill and purge time was also investigated. The measurement cycle is currently dominated by this aspect of the instrument, where increased pressurisation options are presently being explored so that fill/purge times can be reduced. Organic gas species: methane, ethane and propane were also analysed, presenting the opportunity to confirm Raman response linearity with variable gas concentration. Furthermore, multiple gas species were simultaneously detected where each gas component exhibited good peak response linearity. This demonstrated the capacity of the instrument to both detect and reliably quantify gas species where component concentrations varied between 0.04% and >99%. A quantification threshold currently in the order of 100 s ppm is anticipated to increase via incremental procedural and technical developments, making sub-ppm measurements possible within a commercially viable system. Two readily implementable technical developments which would increase instrument limit of detection (LoD) are (a) increasing the Raman excitation laser power (this system operated at approximately 180 mW) and (b) gas sample

pressurisation. Further improvements in the HC-MOF design (such as reduced loss and increased capture efficiency or longer lengths) will also present another opportunity to further increase LoD and/or reduce measurement times.

Future iterations of the instrument will examine these options where LoD in the order of 100 s ppb is predicted. The work described here, therefore aimed to demonstrate the viability of a HC-MOF based Raman gas detection system using relatively low laser power and gas pressure and showcases the use of relatively long fibre lengths to facilitate this, which simultaneously facilitates remote sensing. A clear development path towards increased LoD and reduced measurement time has also been identified.

DATA AVAILABILITY STATEMENT

All data supporting this study are openly available from the University of Southampton repository at https://doi.org/10.5258/SOTON/D1694

ORCID

William S.M. Brooks https://orcid.org/0000-0003-1760-5375
Michael J. Foster https://orcid.org/0000-0001-7833-4500

REFERENCES

[1] L. Mondello, P. Quinto Tranchida, P. Dugo, G. Dugo, *Mass Spec. Rev.* **2008**, *27*(2), 101.

[2] K. Snavely, B. Subramaaniam, *J. Chrom. Sci.* **1998**, *36*(4), 191.

[3] K. Kneipp, H. Kneipp, I. Itzkan, R. R. Dasari, M. S. Feld, *Chem. Rev.* **1999**, *99*(10), 2957.

[4] T. De Beer, A. Burggraeve, M. Fonteyne, L. Saerens, J. P. Remon, C. Vervaet, *Int. J. Pharm.* **2011**, *417*, 1. 32

[5] P. Rostron, S. Gaber, D. Gaber, *Int. J. Eng. Tech. Res.* **2016**, *6*(1), 2321.

[6] C. Rathmell, D. Chen, spectroscopyonline.com, **2018**, *33*, 6, 34.

[7] C. Wen, X. Huang, C. Shen, *J. Raman. Spect.* **2020**, *51*(5), 781.

[8] S. Rupp, A. Off, H. Seitz-Moskaliuk, T. M. James, H. H. Telle, *Sensors* **2015**, *15*, 23110.

[9] M. P. Buric, K. P. Chen, J. Falk, S. D. Woodruff, *Appl. Opt.* **2008**, *47*(23), 4255.

[10] S. Hanf, R. Keiner, D. Yan, J. Popp, T. Frosch, *Anal. Chem.* **2014**, *86*, 5278.

[11] G. T. Jasion, T. Bradley, H. Sakr, J. R. Hayes, Y. Chen, A. Taranta, H. C. Hulvad, I. A. Davidson, N. V. Wheeler, E. N. Fokoua, W. Wang, D. J. Richardson, F. Poletti, *Proc. of SPIE* **2020**, 11309, 1130901–1130902.

[12] G. T. Jasion, J. R. Hayes, N. V. Wheeler, Y. Chen, T. D. Bradley, D. J. Richardson, F. Poletti, *Opt. Exp.* **2019**, *27*, 15.

[13] F. Yang, W. Jin, Y. Lin, C. Wang, H. Lut, Y. Tan, *J. of Lightwave. Tech.* **2017**, *35*(16), 3413.

[14] D. J. Richardson, N. V. Wheeler, Y. Chen, J. R. Hayes, S. Sandoghchi, G. T. Jasion, T. D. Bradley, E. N. Fokoua, Z. Lui, R. Slavik, P. Horak, M. N. Petrovich, F. Poletti, *IEEE Opt. Fib. Comms. Conf. And Expo.* **2017**, Tu3H.1. https://doi.org/10.1364/OFC.2017.Tu3H.1

[15] N. V. Wheeler, M. G. Pappa, T. D. Bradley, Y. Chen, W. Brooks, J. Storey, M. Foster, D. J. Richardson, M. N. Petrovich, *IEEE SENSORS*, Vol. 2017, Glasgow, United Kingdom **2017** 1. https://doi.org/10.1109/ICSENS.2017.8233880

[16] A. Knebl, R. Domes, D. Yan, J. Popp, S. Trumbore, T. Frosch, *Anal. Chem.* **2019**, *91*, 7562.

[17] S. Hanf, T. Bogozi, R. Keiner, T. Trosch, J. Popp, *Anal. Chem.* **2015**, *87*, 982.

[18] T. Jochum, L. Rahal, R. J. Suckert, J. Popp, T. Frosch, *Analyst* **2016**, *141*, 2023.

[19] D. Richardson, Y. Chen, E. Numkum Fokoua, N. V. Wheeler, N. Baddela, J. Hayes, S. Sandoghchi, G. Jasion, J. Wooler, D. Gray, M. Petrovich, F. Poletti, *Specialty Opt. Fib.* **2014**, # SoM4B.1.

[20] I. A. K. Davidson, M. C. Partridge, J. R. Hayes, Y. Chen, T. D. Bradley, H. Sakr, S. Rikimi, G. T. Jasion, E. N. Fokoua, M. N. Petrovich, F. Poletti, D. J. Richardson, N. V. Wheeler, *The Sixth International Workshop on Specialty Optical Fibers and Their Applications (WSOF 2019)*6th–8th Nov., SPIE Digital Library, Charleston, United States **2019** 11206.

[21] G. T. Jasion, T. D. Bradley, K. Harrington, H. Sakr, Y. Chen, E. N. Fokoua, I. A. K. Davidson, A. Taranta, J. R. Hayes, D. J. Richardson, F. Poletti, *Optical Fiber Communication Conference Postdeadline Papers*, Optical Society of America, 2020, Washington DC **2020** paper Th4B.4.

[22] R. Wynne, B. Barabadi, *Appl. Opt.* **2015**, *54*(7), 1751.

[23] E. A. J. Marcatili, R. A. Schmeltzer, *Bell Syst. Tech. J.* **1964**, *43*(4), 1783.

[24] M. Partridge, I. A. Davidson, W. Brooks, M. Foster, T. D. Bradley, J. R. Hayes, G. T. Jasion, M. N. Petrovich, F. Poletti, D. J. Richardson, N. V. Wheeler, in *Seventh European Workshop on Optical Fibre Sensors*, (Eds: K. Kalli, G. Brambilla, S. O. O'Keeffe) Proceedings of SPIE Vol. 11199, SPIE, Bellingham, WA **2019**.

[25] J. Henningsen, J. Hald, *Appl. Opt.* **2008**, *47*(15), 2791.

[26] B. M. Masum, S. M. Aminossadati, M. S. Kizil, C. R. Leonardi, *Appl. Opt.* **2019**, *58*(4), 963.

[27] I. Dicaire, J.-C. Beugnot, L. Thevenaz, *Appl. Opt.* **2010**, *49*(24), 4604.

[28] M. Partridge, R. Curtis, K. Khodabandehloo, Y. Chen, T. Bradley, N. Wheeler, J.R. Hayes, I.A. Davidson, S. Sandoghchi, M.N. Petrovich, F. Poletti, D.J. Richardson, R. Slavik in *Conference on Lasers and Electro-Optics, San Jose, California, 2019/05/05*, Optical Society of America, in OSA Technical Digest, Washington DC **2019** p. STh1L.2. https://doi.org/10.1364/CLEO_SI.2019.STh1L.2

[29] A. Sieburg, A. Knebl, J. M. Jacob, T. Frosch, *Anal. Bioanal. Chem.* **2019**, *411*, 7399.